Towards the development of an electrochemical biosensor for hCGβ detection

2008 Physiol. Meas. 29 S241

(http://iopscience.iop.org/0967-3334/29/6/S21)

IOP PUBLISHING PHYSIOLOGICAL MEASUREMENT

Physiol. Meas. **29** (2008) S241–S254 doi:10.1088/0967-3334/29/6/S21

Towards the development of an electrochemical biosensor for hCGβ detection

Panagiotis Kassanos[1], Ray K Iles[2], Richard H Bayford[2] and Andreas Demosthenous[1]

[1] Department of Electronic and Electrical Engineering, University College London, London, WC1E 7JE, UK
[2] Department of Natural Sciences, Middlesex University, London, EN3 4SF, UK

E-mail: p.kassanos@ee.ucl.ac.uk

Received 11 January 2008, accepted for publication 11 April 2008
Published 10 June 2008
Online at stacks.iop.org/PM/29/S241

Abstract

The free beta subunit of human-chorionic-gonadotropin (hCGβ) is critical for various aspects of human health. Detection and quantification of this protein are essential during pregnancy as it provides clinicians valuable information regarding the progress of a pregnancy and the health of a foetus. Furthermore, it can be used as a biomarker for gestational trophoblastic disease (GTD), germ cell tumours and some non-trophoblastic gynaecological cancers and common epithelial tumours. Monitoring hCGβ levels is particularly important for patient treatment monitoring and relapse detection especially in GTD. This paper presents an investigation of the characteristics of the first two stages necessary for the development of a bio-impedance hCGβ sensor, using impedance spectroscopy and commercially available microelectrodes. Additionally, electrical equivalent circuit models based on the experimental results of these stages are presented. The biosensor is based on the formation of stable antibody–antigen complexes on golden microband electrodes covered with a layer of a self-assembled monolayer (SAM) or with both SAM and protein G. The preliminary results and analysis relate the interfacial processes and physical structure of the sensor to its electrical behaviour. Finally, preliminary results obtained from the sensor without protein G , which strongly indicate hCGβ detection, are also presented.

Keywords: impedance spectroscopy, bio-impedance, hCGβ, biosensor, microband electrodes

(Some figures in this article are in colour only in the electronic version)

1. Introduction

Sensitive optics-based immunomethods for antigen detection such as enzyme-linked immunosorbent assay (ELISA) have widely been employed in laboratories over the past few decades. Their operation is multistage and complex and time consuming since their analysis time is a distinct entity separate from the capture detection system. Thus, real-time monitoring is often not possible in immunoassay measurement systems. The detection system of many optics-based immunoassays is based on the generation of a coloured product from a colourless substrate by an enzyme system linked to the antigen detector molecules. As with all catalysed reactions the speed of the reaction is proportional to the amount of enzymes present. However, if left to run all would reach the same point of completion (exhaustion of substrate). Thus, for ELISAs to yield data fit for purpose, the catalysed reaction is halted by addition of a denaturation agent (e.g. acid) after a set period of time, which halts any further colorimetric changes. Only when this had occurred can optics-based measurement take place. Furthermore, a series of standards must be run in parallel at the same time and under the same conditions in order to 'read off' the optical data and transform it in to measures of antigen concentration. Thus, such instrumentation systems cannot be calibrated *per se* and can never achieve real-time measurement of analytes.

Optics-based real-time measurement is possible in laser surface plasmon resonance devices, where antibody binding (and dissociation) can be measured as a mass-dependent change in the surface plasmon resonance. However, this technique does not compare in robustness or price to classic immunoassays.

Other non-optics-based measurement methodological approaches for ultra low abundance antigens (such as hormones) include surface acoustic wave devices and the variant of this, the quartz crystal microbalance. They all rely on the fact that accumulation of mass on a crystal alters its resonance properties (but so can pressure and temperature). Quartz is piezoelectric and the relationship between applied voltage and mechanical deformation is well known. Applying alternating current to the quartz crystal will induce highly stable oscillations and a high accuracy in the determination of the resonance frequency. As mass is deposited on the surface of the crystal, the thickness increases; consequently the frequency of oscillation decreases from the initial value. This frequency change can be quantified and correlated precisely to the mass change. Again these are not as robust or cost effective as standard immunoassays.

In recent years there has been an increased interest in the development of electrochemical biosensors. Such biosensors offer the advantages of simplicity, low cost and high miniaturization making them easy to make, disposable and portable. Apart from the above they are also precise; they provide analytical time reduction and a completely label-free detection. There is a quite extensive literature (Wang *et al* 2004, Lasseter *et al* 2004, Neubert *et al* 2002) on biosensor design and analysis as is the range of applications they have been designed for.

In general, biosensors are based on modifying surfaces with specific biomolecules, which enable the detection of specific antigens. The construction of such sensors is a very diverse subject, with groups focusing on the use of stable antibody–antigen systems (Wang *et al* 2004), self-assembled monolayers (SAM) (Dijksma *et al* 2000), aptamers (Cai *et al* 2006) and even sensing directly on a substrate (Smiechowski *et al* 2006). Other groups have investigated more complicated structures in order to improve a sensor's ability to detect, even employing gold nanoparticles (Feng *et al* 2005). The analysis and understanding of the electrical characteristics of these complex interfaces is complicated. The measured signal has contributions from each layer of the biosensor, including the buffer solution used, its concentration, the volume used and the substrate on top of which the biosensor is built.

The research presented in this paper describes a biosensor developed using commercially available gold electrodes for the detection of the pregnancy hormone human chorionic gonadotropin (hCG) and its clinically significant free-beta subunit (hCGβ). Found in blood and urine, the mere detection of hCG/hCGβ is the basis of the pregnancy test and monitoring their levels provides valuable information concerning the progress of pregnancy and the health of a foetus (biochemical pregnancy, ectopic pregnancy and fetal aneuploidy (e.g. Downs syndrome) screening). In addition, it may be used as a cancer biomarker since it is associated with gestational trophoblastic disease (GTD), germ cell tumours (testicular cancer) and some non-trophoblastic gynaecological cancers and common epithelial tumours. Levels of hCG, and in particular free hCGβ, are central to patient treatment monitoring and relapse detection in GTD.

It has been noted that 'utilization of hCGβ as a tumour marker is hampered by a limited availability of sensitive and specific assays' (Stenman *et al* 2006). Most modern assay systems for hCG are optic-based ELISAs and although advances have been made, miniaturization to bedside or even automated/continuous monitoring system of the desired level of sensitivity for cancer care purposes has not yet been achieved. Moving away from optics may solve many of the problems encountered. This paper describes preliminary impedance results obtained from the analysis of the first two steps of a biosensor construction on a golden substrate. Well-defined chemistry was used in order to attach to the substrate a protein G layer, which in turn enabled specific immobilization of anti-hCGβ monoclonal antibodies to be used for the simultaneous capture and quantification of hCGβ. EIS measurements were conducted at each construction step and showed that each layer was individually detectable at a specific frequency band.

2. Methods

2.1. Impedance measurement equipment

Impedance measurements were conducted using a Solartron Impedance/Gain-Phase Analyser 1260 model. The instrument was controlled from a PC, using the Smart software supplied with the analyser. This software only allowed voltage injection. AC signals of 5 mV, 10 mV and 15 mV were applied between the working and counter electrodes. These values were chosen as they are widely used in the literature and since they are much less than 0.5 V known to affect protein binding (Lasseter *et al* 2004). For the same reason, no redox probe was used. The signals applied ranged between frequencies of 5 mHz and 1 MHz (Kassanos *et al* 2007). Figure 1 illustrates the experimental setting.

2.2. Electrodes

The electrodes used were commercially available electrodes purchased from Windsor Scientific. There were four golden microbands fabricated using standard microelectronic technology on a p-doped silicon substrate of a 350 μm thickness and a dielectric constant equal to 12 (see figure 2). In more detail, on top of the substrate there was a substrate oxynitride passivation layer of 200 nm thickness with a dielectric constant equal to 6. Subsequently, there were four titanium (Ti) strips with dimensions 2 mm $\times$ 10 μm $\times$ 10 nm (length $\times$ width $\times$ thickness) each, used as an adhesion layer, on top of which the four gold microbands were deposited, each being 2 mm $\times$ 10 μm $\times$ 250 nm in size. On top there was a final organic polymer passivation layer of 1.8 μm thickness, leaving an open window of 1 mm $\times$ 1 mm exposing 1 mm of the length of each golden microband electrode. This determined the active

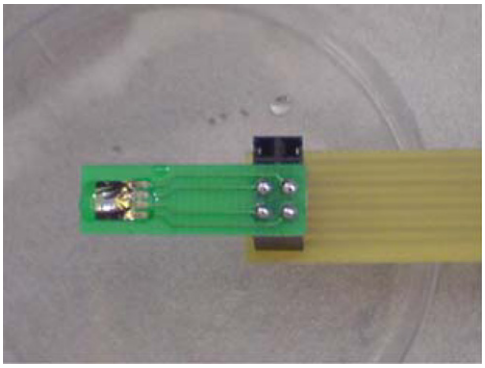

Figure 1. The experimental setting. Close-up of one of the devices used connected to the connector.

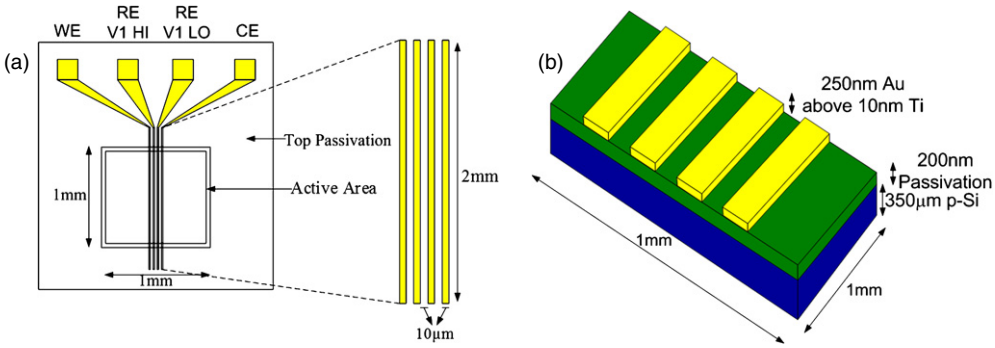

Figure 2. Schematic diagrams of the microband electrodes purchased. In (a) the active area of the sensor, i.e. the non-passivated region, is within the square region of 1 mm × 1 mm dimensions. Also shown in (a) are the connections to the impedance analyser. (b) Not-to-scale representation of the active region of the sensor, not showing the final passivation around it for clarity purposes.

area of the device. Each microband is individually addressable and the distance between each neighbouring microband was 10 μm, the same as their width. All microbands were coplanar and parallel to each other. A not-to-scale figure is shown in figure 2. The electrodes were purchased mounted on a printed circuit board (PCB) with 8 mm width and 25 mm length (see figure 1). The PCB had four gold-plated pins used to connect the PCB to a PCB connector specially designed for these electrodes shown in figure 1. The connector was used to connect each microband to the appropriate BNC socket of the impedance analyser. The first electrode was treated as the working electrode (WE), at which the generator output of the impedance analyser was connected. The fourth electrode was used as the counter electrode (CE) and was connected to the current input BNC socket of the instrument. The second and third electrodes were used as the reference electrodes (RE) and were connected to the V1 Hi and V1 Lo BNCs of the instrument, respectively. A shielding box was additionally used in order to provide shielding to the electrodes to protect the measurements from external electromagnetic noise.

2.3. The biosensor

The biosensor was developed on the active area of the device. On top of the microbands, a self-assembled monolayer (SAM) was developed as described by Neubert *et al* (2002) and at each stage, impedance measurements were made.

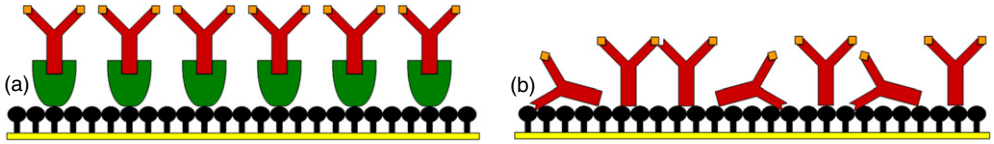

Figure 3. The biosensor developed. (a) With the protein G layer. From bottom to top: the golden substrate, SAM layer, protein G layer and antibodies with attached hCGβ; (b) the sensor without the protein G layer illustrating its reduced detection ability.

The initial layer introduced a protein coupling reactive sulfur residue via dissociative chemisorbtion of the diakyl disulfide, dithiobis succinimidyl propionate (DTSP—Sigma, Poole, UK): 0.5 μl of DTSP (10 mM in anhydrous DMS0—BDH, Poole, UK) was added directly to the gold surfaces of the sensor and was left to incubate at room temperature for 2 h. This was then flood washed with 5 ml of ethanol followed by 5 ml of de-ionized water and then was washed with 5 ml PBS.

The next layer was coupling of recombinant protein G which allows correct orientation of antibodies as shown in figure 3. 0.5 μl of recombinant protein G (Calbiochem, Nottingham, UK), at a concentration of 0.5 μg ml^{-1} was allowed to react freely for 16 h at room temperature in order to achieve covalently immobilized to the gold surface via the DTSP SAM. This was then flood washed with 5 ml of de-ionized water and then washed with 5 ml of PBS.

Finally, anti-hCGβ monoclonal antibodies were specifically immobilized/captured via its Fc domain by the protein G layer. 0.5 μl of McAb anti-hCGb4 (Serotec Ltd, Oxford, UK) (100 μg ml^{-1} in PBS) was added and was allowed to react freely for 16 h at room temperature. This was then flood washed with 5 ml of de-ionized water and then washed with 5 ml of PBS.

The required binding orientation of protein G ensures that all the Fab binding domains of the antibody are pointing away from the sensor surface and thus free to react with target antigens. Thus, increasing the loading capacity of the sensor surface as well as its sensitivity to antigens. Additionally, this highly improves the reproducibility of the sensor, since the antibodies do not attach randomly on the sensor surface. In some of the sensors the protein G layer was not added, in order to test the effect of the protein G layer. Figure 3 shows a schematic side view of the sensor with and without the protein G layer.

2.4. Impedance measurements and biosensor testing

Phosphate buffered saline (PBS) was placed on top of the active region of the sensor at each measurement, in order to hydrate the biosensor, keep the pH constant at 7.4 and maintain physiological conditions. PBS (0.5 μL) was placed on the sensor using a micro-pipette, in order to conduct all the experiments with the same amount of conductive solution on top of the sensor.

In the final test of the antibody-coupled biosensors, 0.5 μl of recombinant hCGβ (Sigma, Poole UK) at a concentration of 250 ng ml^{-1} was added to the sensor surface and allowed to react freely for 16 h at 4 °C. This was then flood washed with 5 ml of de-ionized water and then washed with 5 ml of PBS before impedance was measured as described above.

2.5. Modelling

The experimental data were fitted to electrical equivalent circuits developed using the EIS spectrum analyser (EISSA) software developed by Bondarenko and Ragoisha (2008). Detailed

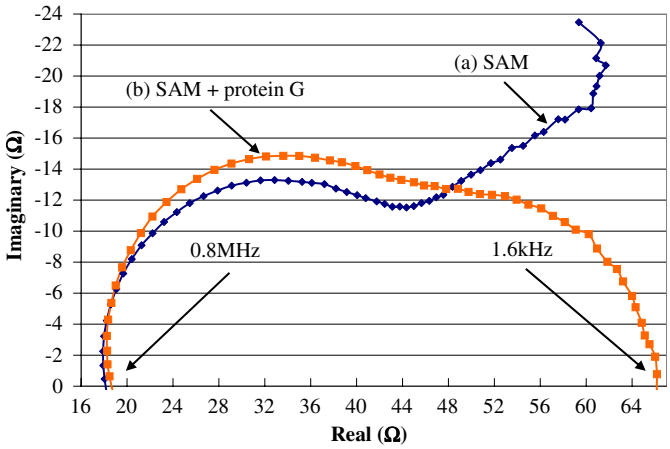

Figure 4. Nyquist plot of the average values of the real and imaginary parts of the impedance when applying a 5 mV signal between WE and CE between 1.6 kHz and 0.8 MHz of the (a) second sensor with just the SAM layer, and (b) third sensor with both the SAM and protein G layers.

description of the operation of this fitting software as well as of the provided equivalent circuits and circuit elements (constant phase element (CPE) and Warburg element) may be found in Bondarenko and Ragoisha (2008).

Circuit (b) of figure 6 is the most standard circuit used in electrochemistry, which is also known as the Randles equivalent circuit. R_{SOL} is a resistor modelling of the buffer solution resistance, C_{dl} is a capacitor used to model the double layer capacitance and R_{CT} models the charge transfer through C_{dl}. The Warburg element is used to model diffusion-limited processes and is used when such characteristics are available, a process which dominates at low frequencies. Another element commonly used in electrochemistry for equivalent circuit fitting is the CPE. The last two elements are non-realistic circuit elements, developed to provide better quality fits, since electrochemical processes do not behave the same way as electronic devices do. The real ($\mathrm{Re}(Z(\omega))$) and imaginary ($\mathrm{Im}(Z(\omega))$) parts of a Warburg impedance (Bondarenko and Ragoisha 2008), which describes semi-infinite diffusion, are given by the following equations:

$$\mathrm{Re}(Z(\omega)) = \frac{A_w}{\sqrt{\omega}} \tag{1}$$

$$\mathrm{Im}(Z(\omega)) = -\frac{A_w}{\sqrt{\omega}}, \tag{2}$$

where A_w is the Warburg coefficient given by

$$A_w = \frac{RT}{n^2F^2A\sqrt{2}}\left[\frac{1}{\sqrt{D_O}C_{S,O}} + \frac{1}{\sqrt{D_R}C_{S,R}}\right], \tag{3}$$

where R is the universal gas constant ($R = 8.314\,472$ J K^{-1} mol^{-1}), T is the absolute temperature, n is the number of electrons, A is the electrode surface area, D is the diffusion coefficient of the electro-active species and C_S is the surface concentration of the species. The subscripts O and R stand for the oxidized and reduced forms of the species.

The impedance of a CPE (Bondarenko and Ragoisha 2008) is given by

$$Z_{\mathrm{CPE}}(\omega) = \frac{1}{Q(\mathrm{j}\omega)^n}, \tag{4}$$

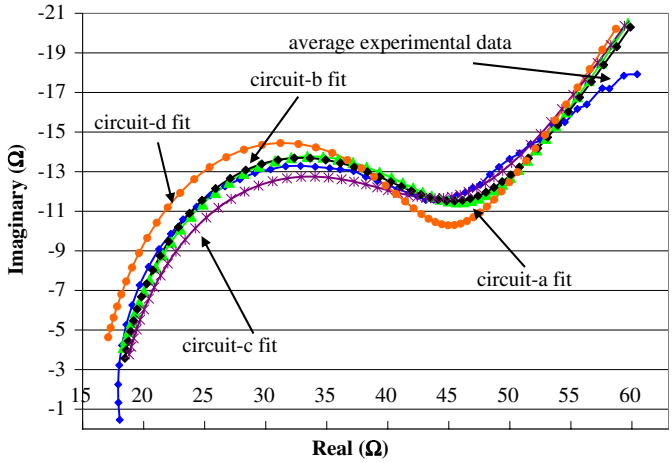

Figure 5. Comparing experimental average data obtained from the sensor with the SAM layer only, with the data obtained from the equivalent circuit-fitting process. These curves refer to circuits shown in figure 6.

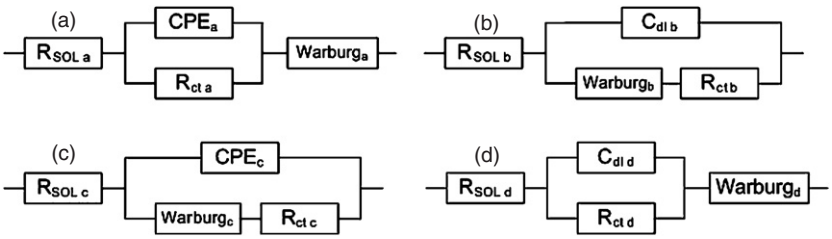

Figure 6. Circuits used to fit the EIS data from the second sensor.

where Q and n are frequency-independent parameters. For $n = 1$ a CPE behaves as an ideal capacitor and for $n = 0$ it behaves as an ideal resistor.

3. Results

Five microband electrodes were used for the measurements described in this paper. The first set of microband electrodes (sensor A) was used without any biological layers on its surface and just with PBS. The second sensor had only the SAM layer developed while the other three sensors had the additional protein G layer on top of the SAM.

Initially 5 mV measurements were conducted between 5 mHz and 1 MHz using the first three PCB mounted sets of electrodes to investigate and find the frequency band giving sensible and useful information. At frequencies below 1 kHz the impedance fluctuated quite randomly, and therefore, the following measurements were conducted within the 1 kHz to 1 MHz frequency band. Each measurement was repeated three times and the average value of the experimental data was calculated. Following this, the average real and imaginary parts of the impedance were plotted against each other and the resulting figure, comparing the results

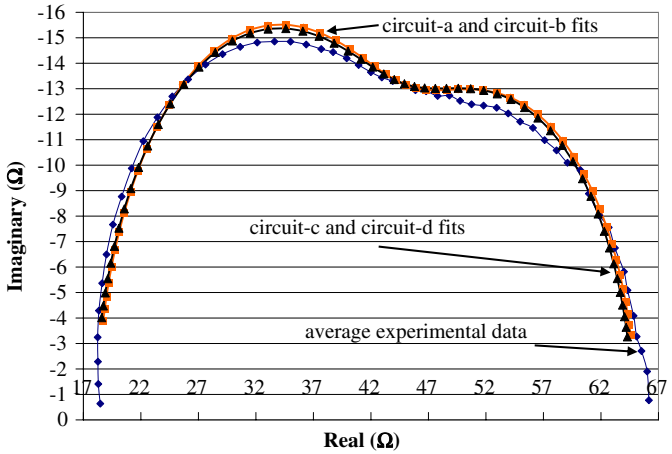

Figure 7. Comparing experimental average data obtained from the sensor with both the SAM and the protein G layer, with the data obtained from the equivalent circuit-fitting process. Results obtained from circuits (a) and (b) and from circuits (c) and (d) overlapped and therefore each pair was combined to a single curve. These curves refer to circuits shown in figure 8.

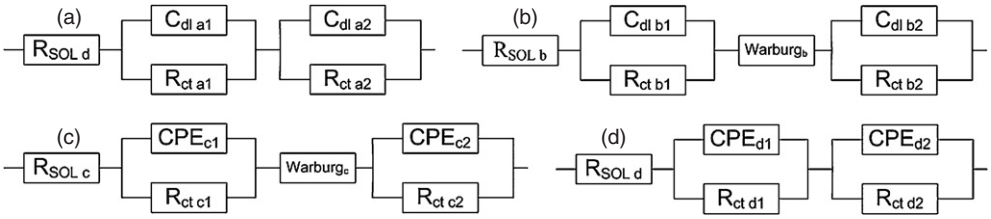

Figure 8. Circuits used to fit the EIS data from the third sensor.

of the sensor with the SAM (sensor B) and the sensor with both the SAM and the protein G layer (sensor C), is shown in figure 4.

The experimental data illustrated in figure 4 were subsequently fitted in equivalent circuit models, using the EISSA software. Figures 5 and 7 show the data obtained from the circuit models, in comparison to the experimental data, while figures 6 and 8 show the circuits used to fit the data, with their respective estimated values listed in tables 1 and 2.

The normalized percentage change of the impedance magnitude from the experimental impedance data of the sensor having just the SAM layer and the sensor, having both the SAM and protein G layer, was calculated and plotted as a function of frequency as shown in figure 9. The data plotted in figure 9 were computed using

$$\frac{Z(\mathrm{SAM}) - Z(\mathrm{SAM} + \mathrm{Protein}\ G)}{Z(\mathrm{SAM})}. \tag{5}$$

The above experiments and analyses were subsequently conducted for 10 mV and 15 mV input signals within the same frequency range. The results from these experiments comparing them with the 5 mV ones are shown in figure 10.

Table 1. Equivalent circuit element values obtained from fitting the second sensor's EIS data. The last two columns show the normalized fitting errors of the solution for the unweighted real and imaginary parts.

Circuit	R_{SOL} (Ω)	R_{SOL} error%	R_{CT} (Ω)	R_{CT} error%	Warburg coefficient (Ω $s^{-0.5}$)	Warburg error%
(a)	16.552	2.4418	23.419	2.4229	2348.2	3.4418
(b)	17.939	1.6735	24.019	1.775	2277.9	2.822
(c)	17.852	5.2804	24.256	1.0651	2266.9	6.276
(d)	15.485	3.5572	23.419	4.0536	2348.2	9.5821
Circuit	C (F)	C error%	CPE Q	Q error%	CPE n	n error%
(a)	N/A	N/A	1.6654×10^{-7}	6.5142	0.93602	0.49934
(b)	5.46×10^{-8}	4.0777	N/A	N/A	N/A	N/A
(c)	N/A	N/A	1.298×10^{-7}	2.8518	0.93796	0.27901
(d)	5.46×10^{-8}	2.6762	N/A	N/A	N/A	N/A
Circuit	r^2 Im($Z(\omega)$)	r^2 Re($Z(\omega)$)				
(a)	1.2583	0.442 08				
(b)	0.86678	0.299 11				
(c)	1.1232	0.9192				
(d)	2.8	1.1485				

Table 2. Equivalent circuit element values obtained from fitting the third sensor's EIS data.

Circuit	R_{SOL} (Ω)	R_{SOL} error%	R_{CT1} (Ω)	R_{CT1} error%	R_{CT2} (Ω)	R_{CT2} error%	Warburg coefficient (Ω $s^{-0.5}$)	Warburg error%
(a)	18.227	2.0797	26.944	1.8204	19.86	3.9878	N/A	N/A
(b)	18.227	2.2996	19.86	4.4114	26.944	2.0124	6.4321×10^{-10}	>1000
(c)	18	3.3758	26.944	3.1583	19.815	6.8815	2.1363×10^{-14}	>1000
(d)	18	3.0148	26.939	2.7921	19.815	6.5028	N/A	N/A
Circuit	C_1 (F)	C_1 Error%	C_2 (F)	C_2 Error%	CPE Q_1	Q_1 Error%	CPE n_1	n_1 error%
(a)	5.4301×10^{-8}	5.1339	7.6546×10^{-7}	7.0892	N/A	N/A	N/A	N/A
(b)	7.6546×10^{-7}	7.8774	5.4301×10^{-8}	5.695	N/A	N/A	N/A	N/A
(c)	N/A	N/A	N/A	N/A	6.0691×10^{-8}	7.431	0.9904	0.56419
(d)	N/A	N/A	N/A	N/A	6.0691×10^{-8}	6.9411	0.99038	0.52818
Circuit	CPE Q_2	Q_2 error%	CPE n_2	n_2 error%	r^2 Im($Z(\omega)$)	r^2 Re($Z(\omega)$)		
(a)	N/A	N/A	N/A	N/A	1.1464	0.4282		
(b)	N/A	N/A	N/A	N/A	1.1699	0.43678		
(c)	7.8867×10^{-7}	8.8175	0.99517	0.78087	1.2462	0.52065		
(d)	7.8236×10^{-7}	8.8609	0.99517	0.7859	1.2187	0.51014		

Subsequently, an anti-hCGβ antibody layer was added on top of the sensors and measurements were conducted. Following this, hCGβ was added on the sensors. The measurements were again conducted after the appropriate incubation times. Figure 11 illustrates the preliminary results obtained from the sensor with no protein G.

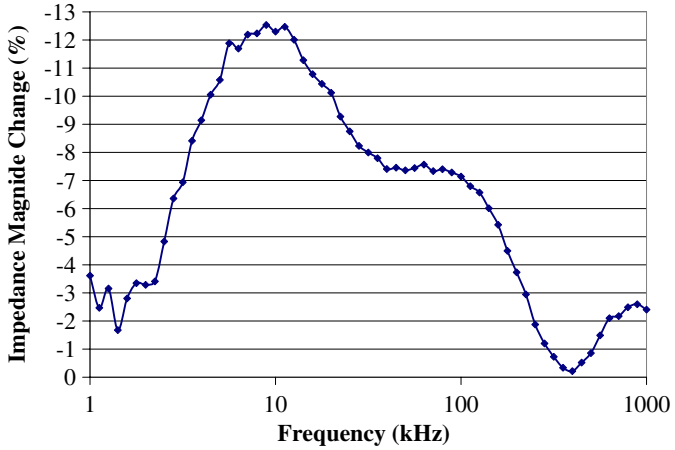

Figure 9. Normalized impedance magnitude percentage change between the average impedance of the sensor with the SAM and that with both the SAM and protein G between 1 kHz and 1 MHz for a 5 mV input signal.

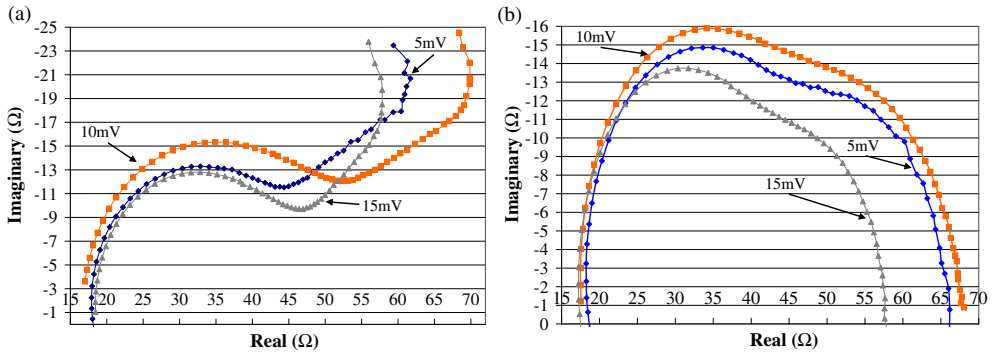

Figure 10. Comparing impedance data acquired when applying 5 mV, 10 mV and 15 mV to the (a) second sensor with the SAM layer only and (b) third sensor with both the SAM and protein G layers between 1 kHz and 1 MHz.

Using the magnitude of the impedance obtained from sensor B up to the antibody level and after hCGβ addition and using equation (6), the normalized percentage change of the impedance magnitude was calculated. This is plotted as a function of frequency in figure 12:

$$\frac{Z(\text{SAM} + \text{Antibodies}) - Z(\text{SAM} + \text{Antibodies} + \text{hCG}\beta)}{Z(\text{SAM} + \text{Antibodies})}. \tag{6}$$

4. Discussion

Figure 4 shows two curves: (a) showing the EIS data of the sensor with the SAM layer (sensor B) and (b) showing the data of the sensor with the SAM and the protein G layer

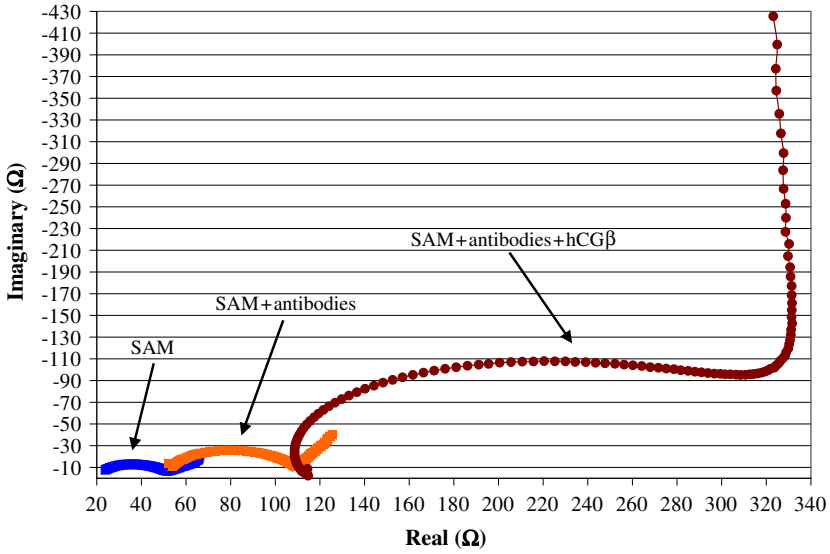

Figure 11. Comparing the EIS data of sensor *B* (the no protein G sensor) for frequencies between 1 kHz and 1 MHz.

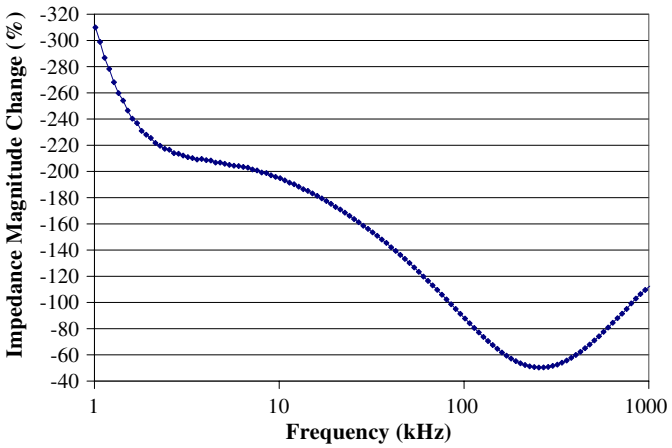

Figure 12. Normalized impedance magnitude percentage change between the average impedance magnitude of the sensor up to the antibody level and that with the addition of hCGβ, between 1 kHz and 1 MHz for a 5 mV input signal.

(sensor C). These two curves are quite distinct from each other. Curve (a) appears to have a semicircular trend until about 25 kHz. After point (43.115, −11.57), the process dominating is a diffusion-limited type with the Nyquist plot suddenly increasing linearly according to

$$y = -0.4252x + 7.5625. \tag{7}$$

Using linear regression, an $R^2 = 0.9918$ was obtained. The slope of this straight line with the x-axis was calculated to be approximately equal to -23.43°. This indicates that it is not

a pure diffusion-dominated process in which case the angle would have been equal to around 45°. The curve intersects the x-axis at $x = 18\ \Omega$. The curve at the low frequency end would intersect the x-axis between 46 Ω and 50 Ω if the semicircular trend was not interrupted by the diffusion-like process taking place thereafter. Until around 25 kHz, the second curve (curve (b)) of figure 4 has a similar trend within the same frequency band. After that point it is observed that the diffusion-limited process appearing previously no longer exists, with the curve crossing the x-axis at 66 Ω at a frequency of 1.58 kHz. We believe that this is attributed to the second additional protein G layer. At the high frequency end (i.e. towards the (0, 0) point), it crosses the x-axis at approximately the same point with the SAM-only curve (curve a) of figure 4.

This high-frequency intersection of both curves at approximately 18 Ω can be attributed to the buffer solution resistance, R_{SOL}. The high-frequency intersection was also used to calculate an approximate value for the charge transfer resistance, R_{CT}, by subtracting from that value the solution resistance. By doing so, the R_{CT} of the SAM only curve was estimated to be equal to approximately 30 Ω, if diffusion is ignored. For the second plot (curve (b) of figure 4) finding R_{CT} is more complicated since the curve is the envelope of two overlapping semicircles. However, if it was treated as a single semicircle, the R_{CT} would be around 48 Ω. Precise calculation of these is not necessary, however these estimates, derived from the graphical analysis of curves (a) and (b) of figure 4, are important as they may serve as rough initial values, required for the circuit-fitting process.

Using these values and the EISSA software, a number of equivalent circuits were developed, for each of these biosensor development stages. These are shown in figures 6 and 8. Initially the fitting began with circuit (a) of figure 6, which did provide a relatively good fit. The initial idea was to build an equivalent circuit as the sensor is being built and hence having started for the sensor B with circuit (a) of figure 6, circuit (c) of figure 8 was subsequently developed. This was, however, proved to be not entirely correct with the other circuits providing better fits, as expected, due to the data of the two sensors differing in the low-frequency region, with sensor C having no diffuse-limited characteristics. This in turn, implies that there is no Warburg element in its equivalent circuit. This was verified by the circuit-fitting software, giving an error of more than 1000% for the Warburg elements of circuits (b) and (c) of figure 8, as shown in table 2. For sensor B circuit (b) of figure 6 appears to provide the best fit. The circuit element values as well as their statistics are shown in table 1. For sensor C, circuit (a) of figure 8 provided the best fit. Circuit element values and statistics are shown in table 2.

Figure 9 indicates that a maximum normalized magnitude percentage change between the sensor with the SAM and the sensor with both the SAM and the protein G layers, of 12.5% is reached at about 9 kHz. The EIS data from figures 10(*a*) and (*b*), which were obtained from experiments conducted with injecting signal amplitudes of 5 mV, 10 mV and 15 mV, have very similar trends between them, with slight changes in frequency range and impedance levels. This indicated as expected that the bioimpedance of the sensor was independent of signal amplitude. The small changes may be attributed to the physiological drift over time.

Figure 11 shows the results from sensor B. It is very clear from this figure that the impedance of the sensor and its characteristics substantially change with the addition of each layer. The real part of the impedance of the SAM layer ranges between 23 Ω and 52 Ω reaching a maximum imaginary part of −12.8 Ω in the semicircular region. The maximum value of the impedance reached in the diffusion-limited region was (65 Ω, −22 Ω). Following the addition of the antibodies, these values change to 52 Ω–110 Ω for the real part and −25.8 Ω for the maximum value of the imaginary part in the semicircular region, with a maximum of (125 Ω, −40 Ω). The addition of hCGβ introduces a dramatic change in these

numbers. The real part was found to be between 108 Ω and 308 Ω with a maximum imaginary part of −225 Ω in the semicircular region. The impedance characteristics seemed then to have a nearly constant real part ranging between 330 Ω and 323 Ω while the imaginary part ranged between −125 Ω and −425 Ω. This region could be modelled by a resistor in series with a capacitor. In addition to the above, figure 12 shows a normalized impedance magnitude percentage change ranging from 350% to 50% within this frequency region between the presence and the absence of hCGβ. Following the above observations, which most importantly show a clear differentiation between the absence and presence of hCGβ, we were led to the conclusion that detection of hCGβ is possible. hCGβ detection using a sensor with protein G is currently being examined. The sensitivity and specificity of the sensor will be examined in the near future.

5. Conclusion

The preliminary results described in this paper show that there is a clear differentiation between different layers of the sensors (figures 4 and 11).

Furthermore, equivalent circuits were developed for two of the sensors, one at the SAM stage of construction and the other at the protein G level. All circuits provided fairly good fits to the experimental data with circuits of figure 6(*b*) (Randles equivalent with Warburg element) and figure 8(*a*) providing the best fits.

More importantly, figures 11 and 12 suggest that hCGβ is detectable, with the EIS data showing a dramatic change after hCGβ addition with a normalized percentage change ranging from 350% to 50%. Even with this commercially available electrode arrays it is possible to detect changes in the electrode interface. However, there is a need to develop an array structure that optimizes the measurement sensitivity. We plan to do this by building on the methodology presented in this paper and by using FEM modelling.

Acknowledgments

We would like to acknowledge the support of the UK Engineering and Physical Sciences Research Council (EPSRC).

References

Bondarenko A S and Ragoisha G A 2008 EIS spectrum analyser www.abc.chemistry.bsu.by/vi/analyser/

Cai H, Lee T M H and Hsing I M 2006 Label-free protein recognition using an aptamer-based impedance measurement assay *Sensors Actuators* B **114** 433–7

Dijksma M, Kamp B, Hoogvliet J C and Bennekom W P 2000 Formation and electrochemical characterization of self-assembled monolayers of thioctic acid on polycrystalline gold electrodes in phosphate buffer pH 7.4 *Langmuir* **16** 3852–7

Feng J J, Zhao G, Xu J J and Hong-Yuan C 2005 Direct electrochemistry and electrocatalysis of heme proteins immobilized on gold nanoparticles stabilized by chitosan *Anal. Biochem.* **342** 280–6

Kassanos P, Iles R K, Bayford R H and Demosthenous A 2007 Development of a biosensor for hCGβ detection *Proc ICEBI XIII-VIII EIT (Graz, Austria, 29 Aug–2 Sept 2007) (IFMBE Proc.* vol 17*)* ed H Scharfetter and R Merwa (Berlin: Springer) pp 620–3

Lasseter T L, Cai W and Hamers R J 2004 Frequency-dependent electrical detection of protein binding events *Analyst* **128** 3–8

Neubert H, Jacoby E S, Bansal S S, Iles R K, Cowan D A and Kicman A T 2002 Enhanced affinity capture MALDI-TOF MS: orientation of an immunoglobulin G using recombinant protein G *Anal. Chem.* **74** 3677–83

Smiechowski M F, Lvovich V F, Roy S, Fleischman A, Fissell W H and Riga A T 2006 Electrochemical detection and characterization of proteins *Biosens. Bioelectron.* **22** 670–7

Stenman U H, Tiitinen A, Alfthan H and Valmu L 2006 The classification, functions and clinical use of different isoforms of hCG *Hum. Reprod. Update* 1–16

Wang M, Wang L, Wang G, Ji X, Bai Y, Li T, Gong S and Li J 2004 Application of impedance spectroscopy for monitoring colloid Au-enhanced antibody immobilization and antibody-antigen reactions *Biosens. Bioelectron.* **19** 575–82